IEEE Access
Multidisciplinary | Rapid Review | Open Access Journal

Received September 25, 2019, accepted October 22, 2019, date of publication November 4, 2019,
date of current version November 14, 2019.

Digital Object Identifier 10.1109/ACCESS.2019.2951418

Insight Into Split Beam Cross-Correlator Detector With the Prewhitening Technique

TIANYU CHEN, YANQUN WU, WEN ZHANG, WEN CHEN, JUN WANG, AND ZHENGLIANG HU

School of Meteorology and Oceanography, National University of Defense Technology, Changsha 410073, China

Corresponding authors: Yanqun Wu (yqwu_nudt@163.com) and Wen Zhang (zhangwen06@nudt.edu.cn)

ABSTRACT The split-beam processing methods have been widely used for the bearing estimation of broadband signals with a line array. They can achieve high bearing resolution at a cost of the reduced processing gain. The split beam cross-correlator detector (SBCD), one of these methods, is to obtain a cross-correlation series from the redundant two-dimensional cross correlations between beam pairs of two sub-arrays. When SBCD is combined with prewhitening techniques in generalized cross correlation (GCC), it shows some unique output characteristics beneficial for both bearing estimation and detection, such as the low output background, the power-independent output, the capacity of accentuating weak targets, suppressing strong interferences, and the resistance to grating lobes aliasing in the spatial spectrum. This paper is to reveal these characteristics and underneath reasons through theories and simulations. Experiment results with an array of 268.75m in South China Sea validate the present theories, and manifest that SBCD with the prewhitening technique can achieve improved performances on both the direction-of-arrival (DOA) estimation and detection of weak broadband targets. In terms of efficiency and robustness for real time applications, it shows great potential in actual underwater environment.

INDEX TERMS Cross-correlator, prewhitening technique, sonar detection, split beam, weak target detection.

I. INTRODUCTION

The split beam process, a classical array processing method, splits a whole array into two sub-arrays and cross-correlates the beam outputs of two subarrays [1]–[7]. One sub-array can be regarded as a hydrophone with increased signal to noise ratio (SNR). It has been shown that the split beam processing is nearly optimal in terms of the direction-of-arrival (DOA) estimation in a spatially incoherent noise environment and provides improved broadband bearing resolution over the full-aperture conventional beamformer (CBF) [6], [8]. Several derived methods have been proposed to improve the DOA estimation and tracking of broadband signals, such as differential cross-correlation method [6], and the cross-spectrum method [9], [10] etc. Nevertheless, Stergiopoulos and Ashley [1] has found that the improved DOA estimation performance of the split beamformer may be practically insignificant by experiments results. What's more, the processing gain of the split beam processing method is 1.5 dB lower than that of the full-aperture CBF [8] (pp. 138–140), and thus its detection performance is reduced [11], [12].

In fact, the cross-correlations between beam pairs of two sub-arrays provide a two-dimensional output of the cross-correlation values versus the steering angles and the time delay between the source and two subarrays. For the incident plane wave, there is a corresponding relationship between the source angle and the resultant time delay between the source and two subarrays. Thus the two-dimensional cross-correlation carries redundant information. Usually, the typical split beam processors in the articles above provide a precise estimation of the target DOA by identifying peaks of the cross correlation at specific beams. In the paper, the split beam cross-correlator detector (SBCD) is presented for the detection of multiple broadband sources, which extracts a cross-correlation series from the two-dimensional output according to the correspondent relationship between the steering angles and the time delays of two beams as the final detection output. The correlation series has a near zero mean output at the noise-only directions, which is beneficial for detection.

Due to the complexity of the ocean environment, the signal and noise spectral characteristics are often nonwhite, which

The associate editor coordinating the review of this manuscript and approving it for publication was Ki-Hong Park.

will cause the associated processing loss of the split beam cross-correlation processing. Miles has examined the effect of signal coherence loss and noise correlation on its detection performance in the presence of frequency-dependent correlated noise fields [12]. The prewhitening techniques are often applied in the generalized cross correlation (GCC) function to improve the performance of time delay estimation [13], [14] in many fields [15]–[17]. The improvement on time delay estimation by the prefiltering techniques and beamforming in the split beam process has also been testified [1] [7]. The role of the prefilters is to enhance the correlation between the two sub-arrays. When SBCD is combined with the prewhitening techniques, the extracted cross-correlation series of the SBCD manifests several different characteristics and presents much better detecting performances. Through analyses in later sections, it has been found by both theories and experimental results that the performances of SBCD with the prewhitening techniques have improved greatly on the DOA estimation and detection of weak broadband targets. The purpose of the paper is to reveal the unique output characteristics of SBCD with the prewhitening techniques and the beneath reasons of these characteristics.

This paper is organized as follows. In Section II, we introduce the process of SBCD and effects of the prewhitening technique through simulations. In Section III, we conduct analysis on the output characteristics of SBCD with prewhitening from four aspects by theories and simulations. In Section IV, we present the real experiments results to confirm the characteristics of SBCD and evaluate its performances in practical applications. In section V, we draw a conclusion.

II. RATIONALE OF SPLIT BEAM CROSS-CORRELATION DETECTOR

A. PROCESS OF SBCD

Without loss of generality, we consider an M-element uniform linear array with the spacing of d to describe the process of SBCD. The angle between the single planar incident wave and the array normal is θ_0 and the steering angle is θ. Neglecting noise and the time factor $e^{-j\omega t}$, the signal of the m-th element is given by

$$X_m(f) = S(f)e^{-j(m-1)\varphi_0}, \tag{1}$$

where $\varphi_0 = 2\pi f d \sin\theta_0/c$ and $S(f)$ denotes the amplitude of signal, and c is sound velocity.

The array is divided into two sub-arrays of $M/2$ elements, and the spacing between two sub-arrays is $\Delta L = (M/2-1)d$. Beams of both sub-arrays are steered with time delays referring to its first sensor. The subscripts x and y denote the left and the right sub-arrays, respectively. Then the normalized beam output of the two sub-array are [18] (pp. 61–62)

$$b_x(f,\theta) = \frac{2}{M}\sum_{m=1}^{M/2} X_m(f)e^{j(m-1)\varphi} = S(f)D(f,\theta,\theta_0), \tag{2}$$

$$\begin{aligned} b_y(f,\theta) &= \frac{2}{M}\sum_{m=M/2+1}^{M} X_m(f)e^{j(m-1)\varphi} \\ &= S(f)D(f,\theta,\theta_0)e^{-j2\pi f\tau_0}, \end{aligned} \tag{3}$$

where $D(f,\theta,\theta_0) = \frac{2\sin(M(\varphi_0-\varphi)/4)}{M\sin((\varphi_0-\varphi)/2)}e^{-j(\varphi_0-\varphi)(M/4-1/2)}$ is the directivity function of an $M/2$-sensor sub-array and $D(f,\theta_0,\theta_0) = 1$. x or y denotes the left or right sub-array and $\tau_0 = -\Delta L\sin\theta_0/c$.

Now we can view two sub-arrays as two receivers spaced by ΔL. Then the cross spectrum $G_{xy}(f)$ is given by

$$\begin{aligned} G_{xy}(f,\theta) &= E\left[b_x(f,\theta)b_y^*(f,\theta)\right] \\ &= e^{j2\pi f\tau_0}E\left[|S(f)|^2\right]|D(f,\theta,\theta_0)|^2. \end{aligned} \tag{4}$$

The cross-correlation time series can be obtained by inverse Fourier transform (IFT)

$$r_{xy}(\tau,\theta) = IFT\left\{G_{xy}(f,\theta)\right\}. \tag{5}$$

Let the time delay be $\widehat{\tau} = -\Delta L\sin\theta/c$. The slice extracted from $r_{xy}(\tau,\theta)$ along $(\widehat{\tau},\theta)$ is the final output of the SBCD. Thus the process of SBCD is equivalent to take the values from the two-dimensional matrix $r_{xy}(\tau,\theta)$ with the $\tau-\theta$ mapping relation of $\tau = -\Delta L\sin\theta/c$. The process flow of SBCD can be summarized by Fig. 1.

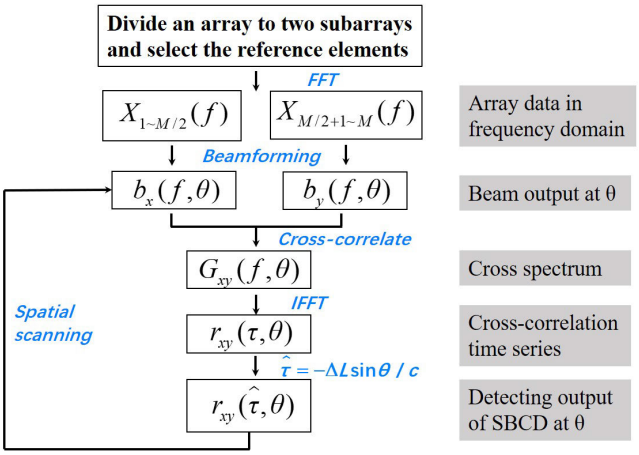

FIGURE 1. The signal processing flow of SBCD.

Here a simulation is conducted to describe the process by adopting a 24-hydrophone uniform linear array with 1 m spacing. A target at 30 degree is band-limited white Gaussian noise of the band 50 ∼ 750 Hz. No prefilter is applied here and no noise considered. Here the white noise is considered as a simple case to illustrate the characteristics of SBCD before and after prewhitening process. All characteristics and results of the SBCD after prewhitening could be applicable to either color noise or other type of broadband signals. In the paper, all the simulation parameters are the same unless otherwise stated.

By the time-shift property of the IFT, the peak value at $\theta = \theta_0, \tau = \tau_0$ is

$$\begin{aligned} & r_{xy}(\tau - \tau_0, \theta_0) \\ &= IFT\left\{e^{-j2\pi f\tau_0} e^{j2\pi f\tau_0} E\left[|S(f)|^2\right] |D(f, \theta_0, \theta_0)|^2\right\} \\ &= IFT\left\{E\left[|S(f)|^2\right]\right\}. \end{aligned} \tag{6}$$

SBCD uses the mapping relation of $\tau = -\Delta L \sin\theta/c$, that is the pink dash curve in Fig. 2 (a), and thus, the output of SBCD without prefiltering represents the power of the target in its direction.

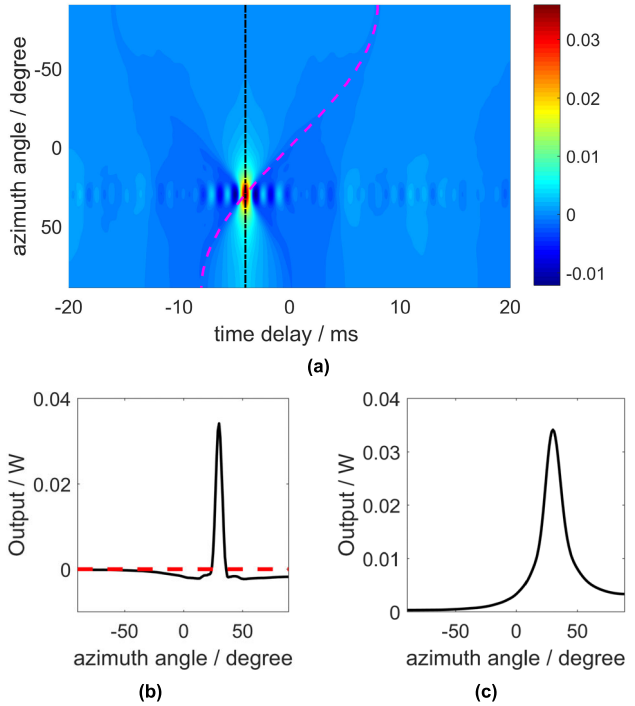

FIGURE 2. (a) Pseudo-color image of $r(\tau, \theta)$ without prefiltering. The pink dash curve corresponds to $\tau = -\Delta L \sin\theta/c$, the black line is at a fixed time delay τ_0. (b) The output of SBCD without prefiltering. The red dash line is the zero-power line. (c) A slice taken at fixed time delay $\tau = \tau_0$.

It's worth mentioning that if $r(\tau, \theta)$ is extracted at a fixed time delay τ_0 (the black line in Fig. 2 (a)), the output is

$$\begin{aligned} & r_{xy}(\tau - \tau_0, \theta) \\ &= IFT\left\{e^{-j2\pi f\tau_0} e^{j2\pi f\tau_0} E\left[|S(f)|^2\right] |D(f, \theta, \theta_0)|^2\right\} \\ &= IFT\left\{E\left[|S(f)|^2\right] |D(f, \theta, \theta_0)|^2\right\}, \end{aligned} \tag{7}$$

which is exactly the CBF result of one sub-array, as is shown in Fig. 2 (c).

In a word, without the prewhitening process, SBCD is also a kind of energy detector.

B. EFFECTS OF THE PREWHITENING PROCESS

The uniqueness of the SBCD with the prewhitening process is shown in this section, and its underlying reasons will be provided in Section III.

Prefiltering techniques are taken as preprocessors in many areas to improve cross-correlations. The GCC function $\widetilde{r}_{xy}(\tau, \theta)$ can be derived by multiplying a prefilter function $W(f)$ with $G_{xy}(f)$ before IFT, that is

$$\widetilde{r}_{xy}(\tau, \theta) = IFT\left\{G_{xy}(f, \theta) W(f, \theta)\right\}. \tag{8}$$

The prewhitening techniques are proposed to suppress the strong tonal noise and the power fluctuation of the target in frequency domain. Smoothed coherence transform (SCOT) [19] is adopted typically in this paper to illustrate the effect of prewhitening, and its weighting function is given by

$$W(f) = \frac{1}{\sqrt{|G_{xx}(f)|}\sqrt{|G_{yy}(f)|}}. \tag{9}$$

The simulation result of SBCD with SCOT is given by Fig. 3. Compared with Fig. 2, there are two key differences after the adoption of prewhitening techniques. The first is the slice of $\widetilde{r}_{xy}(\tau, \theta)$ in Fig. 3 (a) at fixed $\tau = \tau_0$, and the extracted one is shown in Fig. 3 (c). Compared with Fig. 2 (c) it does not comply with the energy space distribution of beamforming in Eq (7). And the output value at the target direction does not represent the power of the target anymore. The second difference is the slice of $\widetilde{r}_{xy}(\tau, \theta)$ extracted by the mapping relation $\tau = -\Delta L \sin\theta/c$, as shown in Fig. 3 (b). The mean value of the output background (the red dash line) is negative and much lower than the background of Fig. 3 (a) which largely is about zero. Because there is a sunken area caught in the two white dash lines in Fig. 3 (a) and the plot of $\tau = -\Delta L \sin\theta/c$ is exactly in this area. Reasons of the two differences will be explained in Section III.

III. PERFORMANCE ANALYSIS OF SBCD AFTER PREWHITENING

A. POWER-INDEPENDENT OUTPUT

The power-independent output characteristic is analyzed, which can explain the first difference without and with prewhitening in Fig. 2 and Fig. 3.

We know a common Fourier transform pair:

$$\delta(n - r) \overset{DFT}{\longleftrightarrow} e^{-jr\Omega}. \tag{10}$$

With Eq. (9) and Eq. (8), the modified cross spectrum after using SCOT can be estimated by the following expression when SNR is big enough to some extent [20] (pp. 191-192):

$$\widehat{G}_{xy}(f) = \frac{1}{\sqrt{|G_{xx}(f)|}\sqrt{|G_{yy}(f)|}} G_{xy}(f) \approx e^{-j2\pi f\tau_0}. \tag{11}$$

The above equation denotes the power-independent characteristics of the output of SBCD with the prewhitening process.

For signals of finite band width, the cross-correlation output $r_{xy}(\tau, \theta_0)$ is expressed by

$$r_{xy}(\tau, \theta_0) \propto B_w \mathrm{sinc}[\pi B_w(\tau - \tau_0)] \cos[2\pi f_0(\tau - \tau_0)], \tag{12}$$

where B_w is the bandwidth of the signal and f_0 is the center frequency.

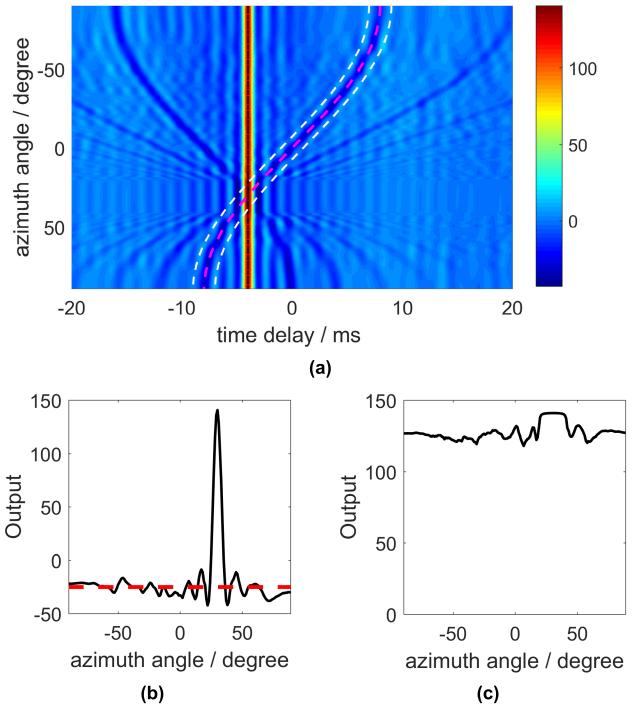

FIGURE 3. (a) Pseudo-color image of $\widetilde{r}_{xy}(\tau,\theta)$ with SCOT. The pink dash curve corresponds to $\tau = -\Delta L \sin\theta/c$, the black line is at a fixed time delay τ_0. (b) The output of SBCD. The red dash line is the mean value of the sidelobes of the SBCD. (c) A slice taken at fixed time delay $\tau = \tau_0$.

It's known the output of the CBF represents the energy in the space. If any parameter of the signal or noise at the sensor varies, its output would change as well. However, from Eq. (12), with the SCOT prewhitening technique, the cross-correlation output of a bandwidth limited signals is proportional to the signal bandwidth. The cross-correlation peak values of the prewhitened SBCD depend on the signal bandwidth and how much the cross-spectrum is whitened. As the desired signal bandwidth increases, the peak value increases, while monochromatic signals will be completely suppressed in SBCD with prewhitening.

To illustrate how the signal bandwidth and SNR influence the output of the prewhitened SBCD, we conducted some simulations with the previous parameters.

Fig. 4 shows the output power of the prewhitened SBCD steered at the target direction versus the input SNR in each channel of the array, where the frequency bandwidths of the target are 300 Hz, 500 Hz and 700Hz, respectively. When the input SNR exceeds 0 dB, the output at the target direction of the prewhitened SBCD will not rise significantly anymore as SNR rises. Therefore, the signal bandwidth decides the ultimate output power of the prewhitened SBCD.

Also, this characteristic explains why the output $\widetilde{r}_{xy}(\tau,\theta)$ in Fig. 3 (c) nearly turns to be nearly flat. When steering at directions away from the target, the energy will decrease. But according to Eq. (11), the cross spectrum will not be influenced by steering angle and the peak value and is only decided by bandwidth after prewhitening. So the values in

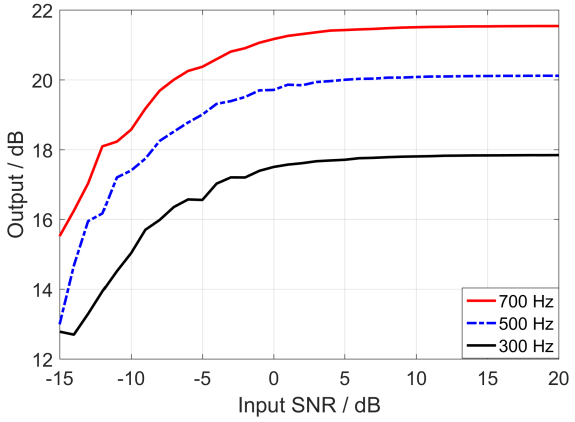

FIGURE 4. The output of the prewhitened SBCD steered at the target direction versus the SNR. Signal frequency bandwidths are 300 Hz, 500 Hz and 700Hz, respectively.

Fig. 3 (c) will not change much as the steering direction changes.

B. NEGATIVE OUTPUT BACKGROUND

The negative output background of SBCD with prewhitening is another important characteristic which contributes to the good performance of SBCD.

From Fig. 3, we know that the values of SBCD output are lower than the background of $\widetilde{r}_{xy}(\tau,\theta)$ at angles $\theta \neq \theta_0$. This phenomenon always exists in simulations and real experiments results, which can be explained as follows.

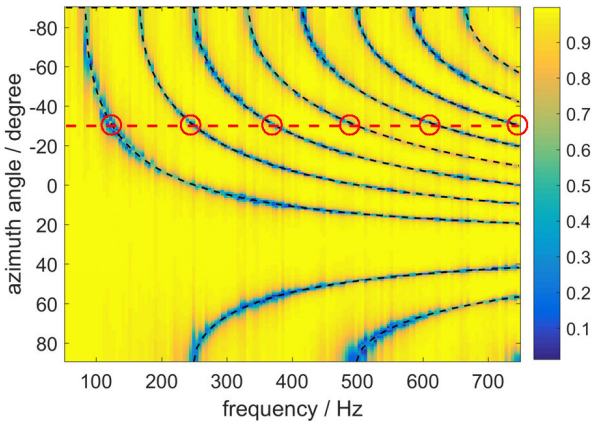

FIGURE 5. Absolute values of cross-spectrum in all steering directions. The red line corresponds to $M(\varphi_0 - \varphi)/4 = k\pi$. The black lines are drawn by $\theta = -30°$ and the red circles are their cross points with the red line.

From Eq (2), the directivity function $D(f,\theta,\theta_0)$ equals zeros when $M(\varphi_0 - \varphi)/4 = k\pi$ where k is an integer. Then the cross-spectrum $G_{xy}(f,\theta) = 0$ in Eq (4). In this case, prewhitening is of no sense. The absolute value of cross-spectrum $\left|G_{xy}(f,\theta)\right|$ in Fig. 3 is examined in Fig. 5 where these black dash curves drawn by the formula $M(\varphi_0 - \varphi)/4 = k\pi$ are in accordance with zeros paths of cross-spectrum. Take the slice in Fig. 5 at $\theta_0 = -30°$

for example. There are six frequency points in the processing frequency band of 50 ∼ 750 Hz making the zero value of the cross-spectrum, which are marked in Fig. 5.

Generate a prewhitened cross spectrum $\widehat{G}_{xy}(f) = e^{-j2\pi f\tau_0}$. The IFT of $\widehat{G}_{xy}(f)$ is shown in Fig. 6 (a).

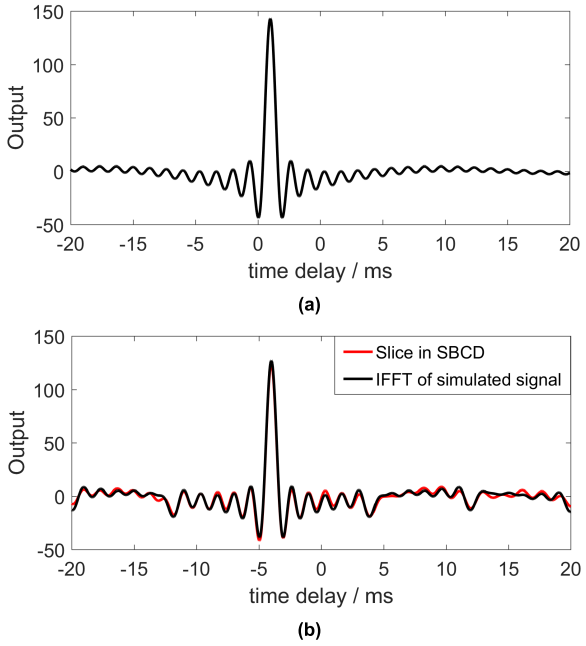

FIGURE 6. (a) IFT of the generated prewhitened cross spectrum $\widehat{G}_{xy}(f)$; (b) IFT of $\widehat{G}_{xy}(f)$ with zeros at six frequency points in Fig. 5 and a slice of Fig. 2 (a) at $\theta = -30°$. The blue dash line indicates the position of the dipped value.

In Fig. 6 (b), if we put $\widehat{G}_{xy}(f)$ at those six frequency points to zero, there will be a series of cyclically dips in the IFT result compared with Fig. 6 (a). The position of these dips match with the slice taken from Fig. 3 (a) at $\theta = -30°$, which is the red dash line in Fig. 6 (b). For different steering angles, dips appear at different points. All dips can be connected to a sunken area like Fig. 3 (a). The curve $\tau = -\Delta L \sin\theta/c$ is just along these values, which means $\widetilde{r}_{xy}(\tau(\theta), \theta)$ is local minimum in terms of τ at angles $\theta \neq \theta_0$, as shown in Fig. 6 (b).

To sum up, the zeros of the directivity function explain why the output background of SBCD is negative. The decline of the background level helps highlight the very weak target. This is an important characteristic of SBCD.

C. ANTI-INTERFERENCE CAPAABILITY

Under real underwater scenarios, a weak target is to be detected against strong interference. The interference would degrade the detection of the weak target. What's even worse, when their directions are extremely close, the energy leakage or sidelobes of the interference will submerge the weak target. The power independent characteristic and negative mean background of the SBCD provide the capability to magnify the weak broadband signals and reduce the strong broadband or tonal interference.

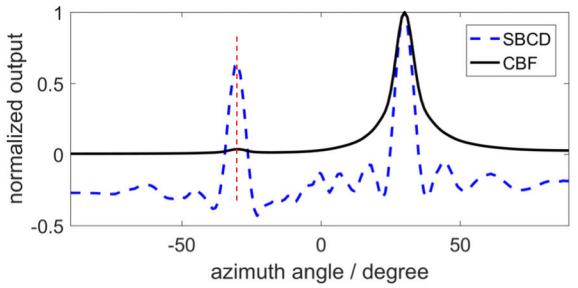

FIGURE 7. The normalized output of CBF (the blue line) and SBCD (the black line). The target is at the direction of −30 degree while the interference 30 degree. The input SIR is −15 dB. The red dash lines indicate the target direction.

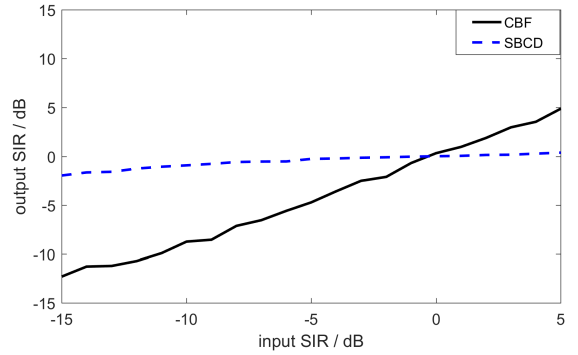

FIGURE 8. Effect of the input SIR on the output SIR by comparison of SBCD with CBF. Conditions are the same as Fig. 7.

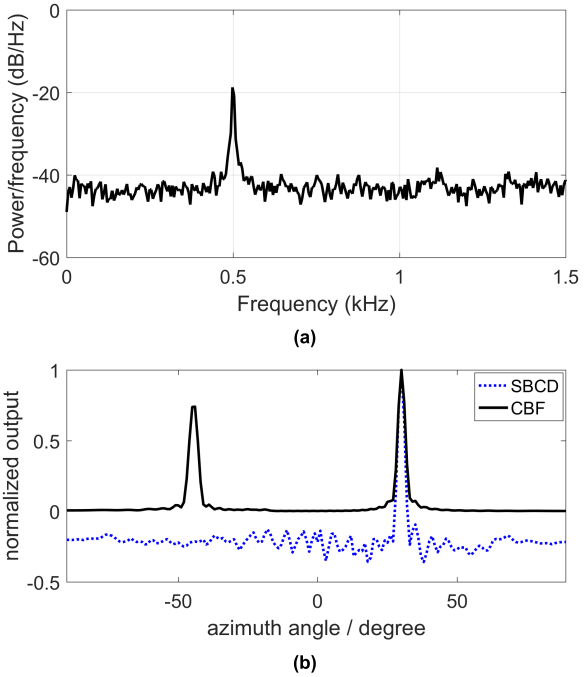

FIGURE 9. (a) The frequency spectrum of the simulated signal. The strong line spectrum is 500 Hz; (b) The output of CBF and SBCD. The target is at the direction of 30 degree.

Simulations are conducted to signify the anti-interference capability of SBCD. In Fig. 7, the normalized output of CBF and SBCD using the whole array are compared. The signal to

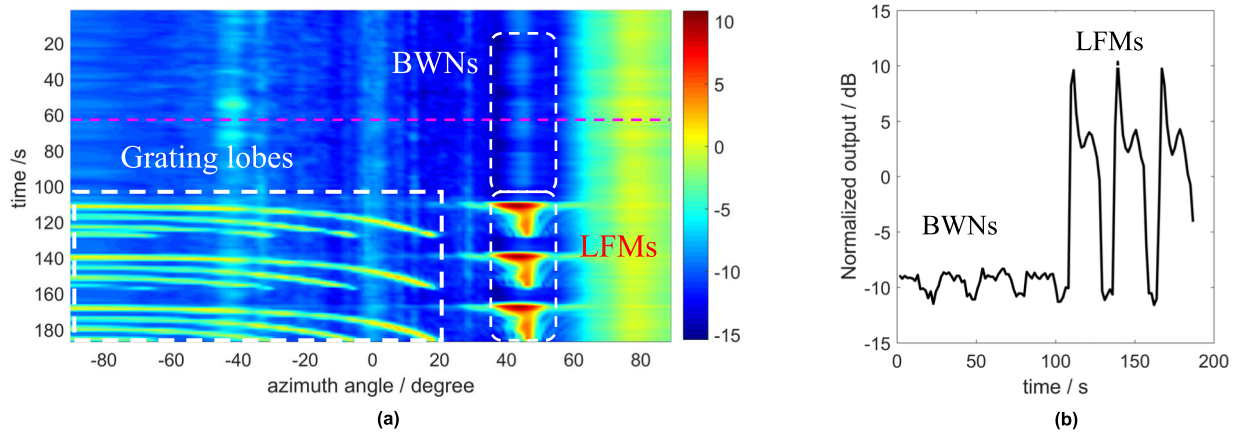

FIGURE 10. Results of CBF in Event 1. (a) BTR diagram in dB. The pink dash line is at the time of 60 s; (b) A slice at the direction of 46 degree.

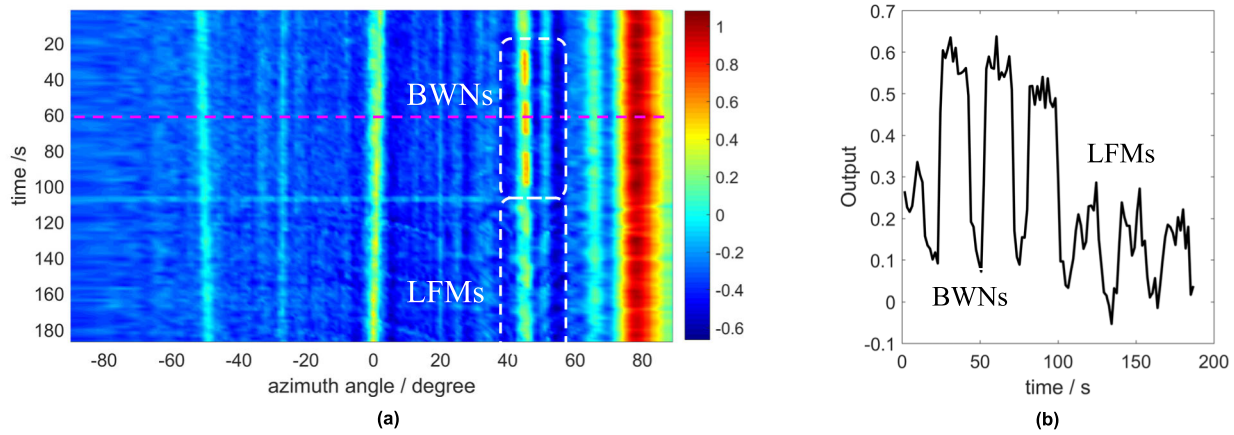

FIGURE 11. Results of SBCD in Event 1. (a) BTR diagram. The pink dash line is at the time of 60 s; (b) A slice at the direction of 46 degree.

interference ratio (SIR) of SBCD is much higher than that of CBF, while the SBCD output value of the weak target is prominent from the background, which means the weak signal can be easily distinguished.

Then the output SIR versus the input SIR is analyzed for both CBF and SBCD, where the CBF utilizes the whole array. In Fig. 8, the output SIR of the CBF nearly remains the same as the input SIR since it presents true power from each direction. By contrast, the output SIR of SBCD improves greatly, but it doesn't change much as the input SIR varies from -15 dB to 0 dB. To sum up, the two simulations verifies that the SBCD has an anti-interference capability due to the power-independent output and the lower output background.

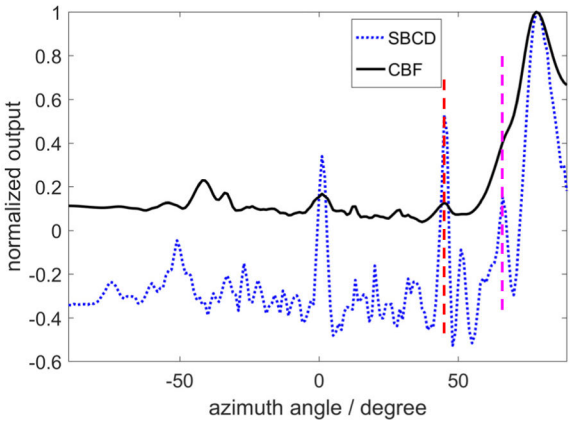

FIGURE 12. Comparisons of results of CBF and SBCD at the time of 60 s. The red dash line and the pink dash line indicate the direction of the transducer (46 degree) and another target to be discussed (66 degree), respectively.

D. RESISTANCE TO GRATING LOBES ALIASING BROUGHT BY LINE SPECTRA

The array spacing is often designed to be $d \leq c/2f_{\max}$ in order to satisfy the spatial Nyquist sampling theorem, where $f_{\max}$ is the maximum working frequency of the array. For the signal with the center frequency f_0 exceeding $c/2d$, the problem of grating lobes aliasing will appear, leading to a set of cyclically ambiguous direction-of-arrival estimates which is mainly brought by tonal signals [21].

Usually, the grating lobes aliasing is mainly caused by strong line spectrum or narrowband part of targets.

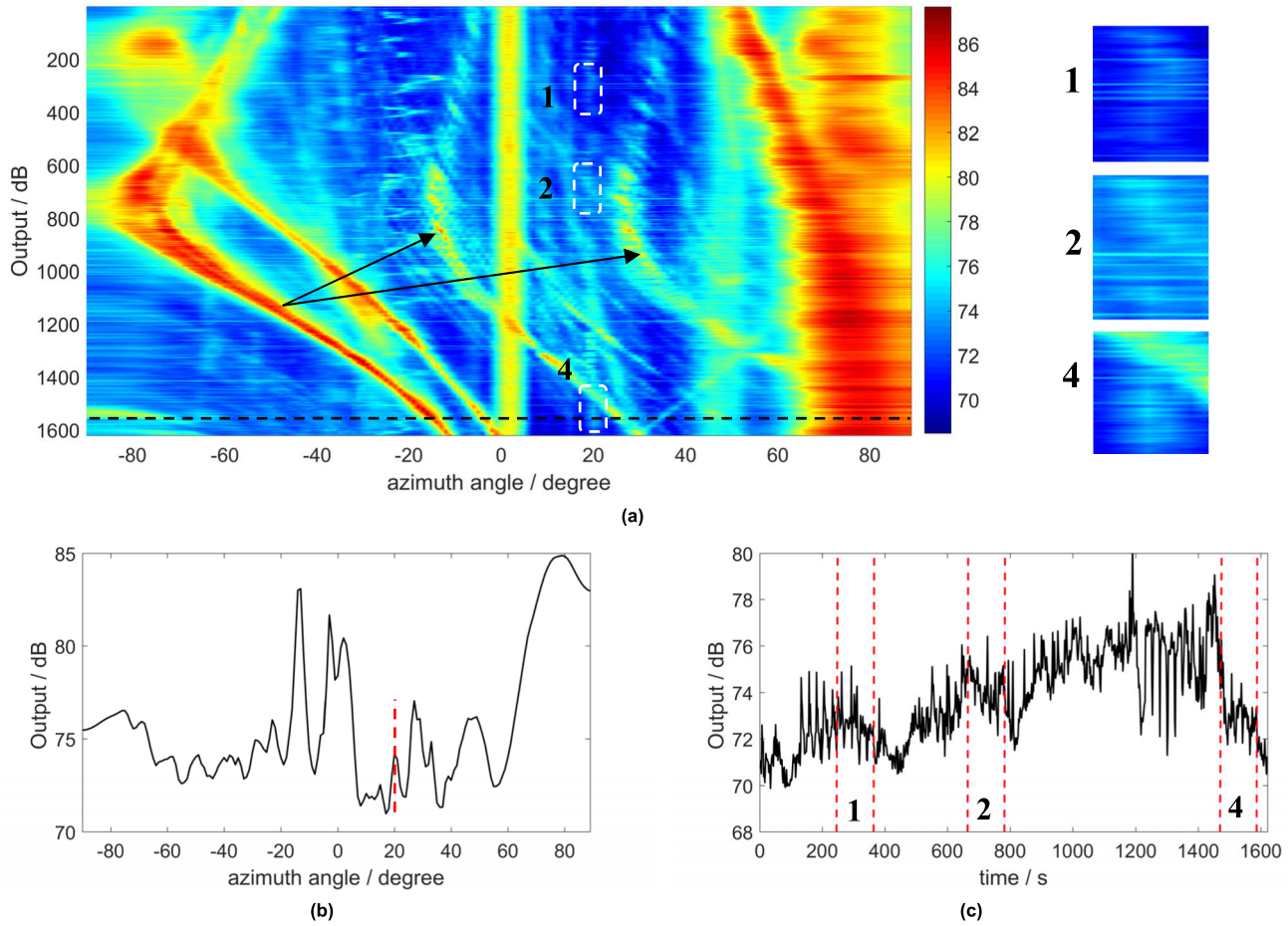

FIGURE 13. Results of CBF in Event 2. (a) BTR diagram in dB. The white lines highlight the position of the transducer. The black line is at the time of 1578s. The two black arrows indicate two grating lobes and their origin target; (b) A slice at the time of 1578 s. The red line indicates the direction of the transducer; (c) A slice along the trace of the acoustic transducer. The time range of white noise pulses are marked by red lines.

Prewhitening process can suppress strong tonal signals and flat the signal power spectrum.

We hereby simulate a typical ship-radiated noise with broadband continuous spectrum and strong line spectrum, which is shown in Fig. 9 (a). Particularly in this simulation, the array spacing is 2.5 m, corresponding to the maximum working frequency of 300 Hz. As expected, there is a fake false target at -30 degree using CBF as shown in Fig. 9 (b), while SBCD does not have such a problem. Overall, SBCD can effectively overcome the problem of grating lobes brought by strong line spectrum of targets

IV. REAL EXPERIMENT RESULTS

In this section, experiment results were analyzed to validate the characteristics of SBCD and its advantages on the detection of broadband signals. The experiment was conducted in an offshore area of Sanya in South China Sea, and a 44-element uniform linear array of 6.25 m sensor spacing was deployed on the ocean bottom. The UW350 transducer carried by a ship generated broadband white noise (BWN) pulses and linear frequency modulation (LFM) pulses. We mainly focus on the detection performances of BWN pulses, which are like real targets.

Data of two events were collected for further analysis. During Event 1, the surface ships near the experiment site was comparatively few, and the data was helpful to validate the characteristics and advantages of SBCD. During Event 2, it was in a heavy traffic environment and the results of SBCD testify its performances under complex conditions.

A. EVENT 1

In this event, the acoustic transducer at 46 degree generated four BWN pulses and LFM pulses at 100 $\sim$ 600 Hz, lasting for 20 s and intermitting for 10s. In this event, the transmitted powers of LMF pulses were around 3$\sim$5 dB higher than BWN pulses. The distance from the transducer to the first hydrophone was only 975 m. Thus each sub-array of 8 elements is adopted here for the plane wave beamforming.

Figs. 10(a) and 11 (a) demonstrate the bearing time recording (BTR) of CBF and SBCD respectively for comparison. In Fig. 10 (a), there are a series of grating lobes together with LFM pulses since the $f_{\max}$ corresponding to the spacing

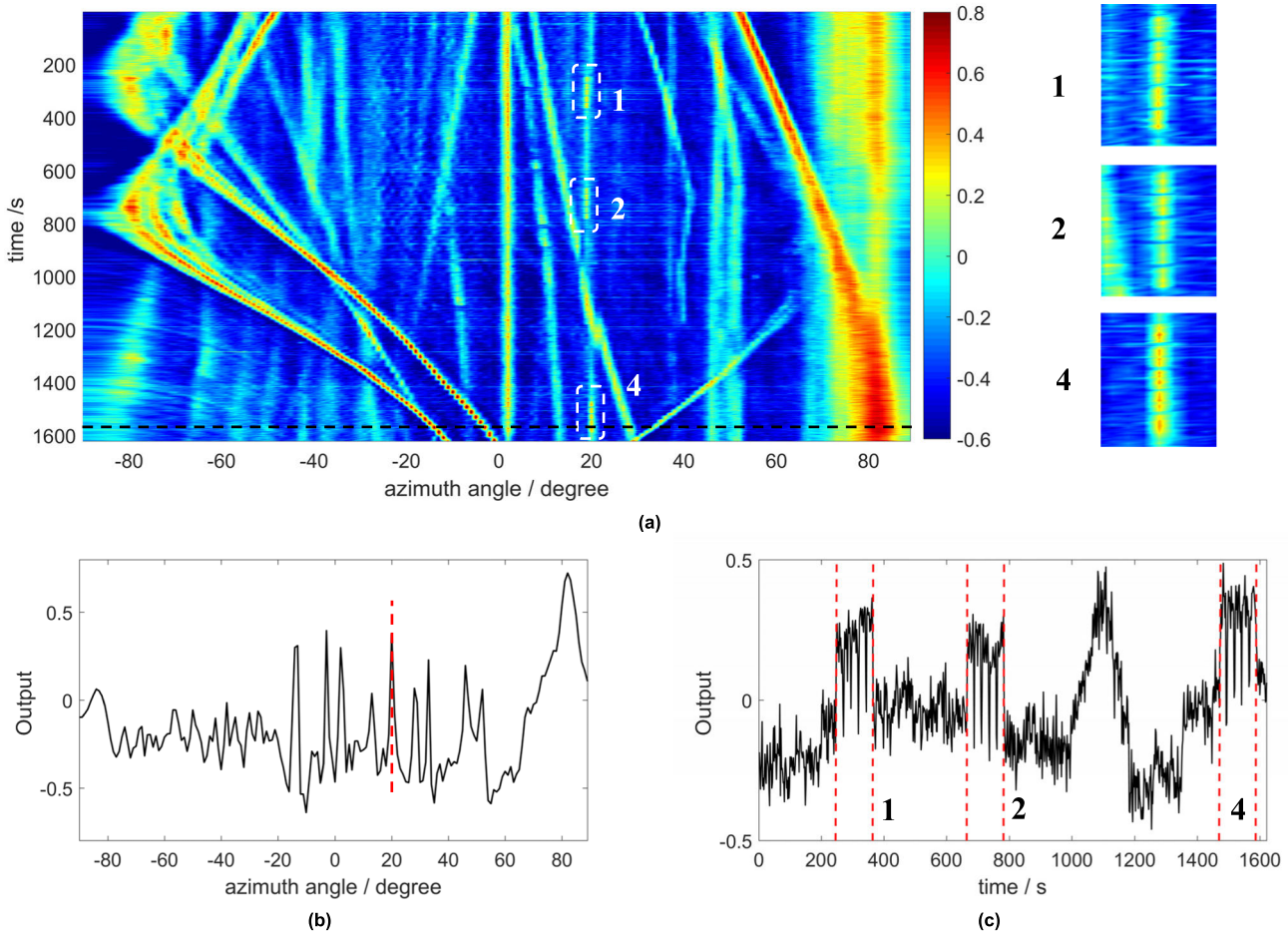

FIGURE 14. Results of SBCD in Event 2. (a) BTR diagram and three enlarged subfigures for three groups of BWN pulses; (b) A slice at the time of 1578 s; (c) A slice along the trace of the acoustic transducer. The symbols in the figure indicate the same information as in Fig. 13.

of 6.25 m is 120Hz. As the frequency of LFM signal changes with the time, the direction of grating lobes changes as well. According to the resistance capability of SBCD to grating aliasing, we can expect the grating lobes are diminished in Fig.11 (a).

When steering beam pairs of two sub-arrays to the direction of the target, the powers of both CBF and SBCD versus time are compared in Figs. 10(b) and 11 (b). It's seen in Fig. 10(b) that powers of LFM are larger than BWN in CBF since CBF reflects the real powers of transmitted signals. However, it's contrary for SBCD as shown in Fig. 11(b). According to its power-independent output characteristics, its output power at the target direction depends on the frequency bands of the target. For the beamforming time of 0.8s (shorter than 20s), the frequency band of LFM signals is very narrow, and thus the outputs of LFM for SBCD are lower than those of BWN.

To further testify the anti-interference capability of SBCD in real data, both results of SBCD and CBF at the time of 60s are extracted for comparison, as shown in Fig. 12. From the recording of Automatic Identification System (AIS) installed in the ship, there was a merchant vessel nearby at around 66 degree at that time (corresponding to the pink dash line in Fig. 12). However, it is submerged in the sidelobes of the strong interference at near 80 degree in the result of CBF, while in the result of SBCD, this vessel is well resolved from the interference. Thus not only weak BWNs are more prominent than those of CBF, but also the invisible vessel becomes visible. What's more, the normalized output background is negative and much lower than that of CBF, which validates the negative output background of SBCD. The results above are the synthetic effects of the power-independent output characteristics and the negative output backgrounds of SBCD.

From the analyses above, all characteristics of SBCD with the prewhitening technique in previous sections have been verified in Event 1.

B. EVENT 2

During Event 2, the distance from the acoustic transducer to the first hydrophone was 3600 m. The transducer at 20 degree generated four groups of pulses. Each group has 5 LFM pulses and 5 BWN pulses. The signal band was 30 $\sim$ 300 Hz and the pulse length was 20 s. The source level of the four pulse groups are respectively 119 dB, 135 dB,

145 dB and 155 dB ref μPa. In this event, there were several strong interferences, which complicated the environment. All 44 hydrophones were used.

Fig. 13 (a) and Fig. 14 (a) give us a bird view of performances of the CBF and SBCD, respectively. Compared with results of CBF in Fig. 13 (a), powers along traces of all detected targets with SBCD in Fig. 14 (a) are balanced and clear. And besides, the BWN pulses can be well identified. While with CBF, signal pulses are almost submerged in the background and other interferences, which means an unfavorable performance for detection.

In Fig. 13 (a), there are two parallel grating lobes like those in Fig. 10 (a). The grating lobes, having messed the background and disturbed the detection, are caused by the strong line spectrum of the striking targets, which are indicated by the two black arrows. This has been confirmed by the disappearance of the aliasing when the processing band is narrowed.

Slices of BTR results at the time of 1578 s, corresponding to the BWN pulse of 155 dB, are taken out as shown in Fig. 13 (b) and Fig. 14 (b). It further confirms that outputs of all broadband targets with SBCD are balanced and thus SBCD has improved the output SIR and SNR.

The bearing series of the acoustic transducer are taken out to further visualize their performances, especially on BWN pulses, which corresponds to the time duration marked between red dashed lines in Fig. 13 (c) and Fig. 14 (c). In Fig. 13 (c), outputs of BWN pulses are approximate to the background. By comparison, Fig. 14 (c) indicates that four groups of five BWN pulses of different source levels are well detected, except that the third group is badly obscured by a loud interference.

Overall, results of Event 1 have testified the theoretical characteristics of SBCD in Section III, and results of Event 2 have not only validated the present theories but also showed its robust performance under real complex environment.

V. CONCLUSION

The paper explored the unique characteristics and special detecting effects of SBCD with the prewhitening technique through theories and experimental results. It's been found that the final output of the cross-correlation bearing series of SBCD is almost independent of the signal power and dependent on the signal bandwidth and the signal spectral characteristics. Consequently, both the target and the strong interference will present comparable peaks in the output of SBCD, which renders its capability of suppressing the strong interference. Moreover, the negative output background of the SBCD caused by zero points of the half-array directivity makes the weak broadband signal identifiable even under loud ambient noise. And it can effectively overcome the problem of grating lobes in the spatial spectrum caused by line spectra of any sources. Experimental results have manifested the SBCD with the prewhitening technique can achieve superior performance in the detection of weak broadband targets. On top of that, SBCD is computational effective and robust, lending its practicality as tested in the real data. All the theories conducted in the manuscript can be generalized for signals of high frequency bands without any efforts.

Last but not least, the beamforming process of SBCD is not limited to the delay-and-sum beamformer in the paper. Other high-resolution method will also be of great interest for our further study.

REFERENCES

[1] S. Stergiopoulos and A. T. Ashley, "An experimental evaluation of split-beam processing as a broadband bearing estimator for line array sonar systems," *J. Acoust. Soc. Amer.*, vol. 102, no. 6, pp. 3556–3563, Jul. 1997.

[2] A. D. George and K. Kim, "Parallel algorithms for split-aperture conventional beamforming," *J. Comput. Acoust.*, vol. 7, no. 4, pp. 225–244, Dec. 1999.

[3] S. E. Fried, S. C. Walker, W. S. Hodgkiss, and W. A. Kuperman, "Measuring the effect of ambient noise directionality and split-beam processing on the convergence of the cross-correlation function," *J. Acoust. Soc. Amer.*, vol. 134, pp. 1824–1832, Aug. 2013.

[4] Z. Torbatian, R. Adamson, M. Bance, and J. A. Brown, "A split-aperture transmit beamforming technique with phase coherence grating lobe suppression," *IEEE Trans. Ultrason., Ferroelectr., Freq. Control*, vol. 57, no. 11, pp. 2588–2595, Nov. 2010.

[5] H. Cao and Z. Cai, "A binning method based on split-beam array to suppress reverberation," in *Proc. IEEE/OES China Ocean Acoust. (COA)*, Jan. 2016, pp. 1–6.

[6] V. H. MacDonald and P. M. Schultheiss, "Optimum passive bearing estimation in a spatially incoherent noise environment," *J. Acoustical Soc. Amer.*, vol. 46, no. 1A, pp. 37–43, 1969.

[7] B. G. Ferguson, "Improved time-delay estimates of underwater acoustic signals using beamforming and prefiltering techniques," *IEEE J. Ocean. Eng.*, vol. 14, no. 3, pp. 238–244, Jul. 1989.

[8] A. D. Waite, *Sonar for Practising Engineers*. Hoboken, NJ, USA: Wiley, 2002.

[9] A. Piersol, "Time delay estimation using phase data," *IEEE Trans. Acoust., Speech Signal Process.*, vol. ASSP-29, no. 3, pp. 471–477, Jun. 1981.

[10] Q. Li, "A precise bearing estimation method of digital split-beam array system," in *Proc. IEEE Int. Conf. Acoust., Speech, Signal Process.*, vol. 11, Apr. 1986, pp. 1817–1820.

[11] G. Carter, "Time delay estimation for passive sonar signal processing," *IEEE Trans. Acoust., Speech, Signal Process.*, vol. 29, no. 3, pp. 463–470, Jun. 1981.

[12] D. A. Miles, D. Kirk, and T. Clarke, "A Statistical Analysis of the Detection Performance of a Broadband Splitbeam Passive Sonar," *IEEE J. Ocean. Eng.*, vol. 31, no. 4, pp. 986–996, Oct. 2006.

[13] G. C. Carter, "Coherence and time delay estimation," *Proc. IEEE*, vol. 75, no. 2, pp. 236–255, Feb. 1987.

[14] C. H. Knapp and G. C. Carter, "The generalized correlation method for estimation of time delay," *IEEE Trans. Acoust., Speech Signal Process.*, vol. 24, no. 4, pp. 320–327, Aug. 1976.

[15] L. Chen, Y. Liu, F. Kong, and N. He, "Acoustic source localization based on generalized cross-correlation time-delay estimation," *Procedia Eng.*, vol. 15, pp. 4912–4919, 2011.

[16] Y. Liu, Y. Tie, D. Li, and S. Na, "Leak detection and location using generalized correlation time delay estimation algorithm," *Adv. Mater. Res.*, vol. 482, pp. 1741–1746, Feb. 2012.

[17] A. H. Yahia, E. S. El-Dahshan, and A. K. Guirguis, "Time delay estimation, using correlation approaches applied to seismic time picking," *J. Appl. Geophys.*, vol. 10, no. 1, pp. 1–10, Jan. 2018.

[18] S. N. Prabhakar, *Sensor Array Signal Processing*, 2nd ed. Boca Raton, FL, USA: CRC Press, 2009.

[19] G. C. Carter, A. H. Nuttall, and P. G. Cable, "The smoothed coherence transform," *Proc. IEEE*, vol. 61, no. 10, pp. 1497–1498, Oct. 1973.

[20] J. Benesty, J. Chen, and Y. Huang, *Microphone Array Signal Processing* (Springer Topics in Signal Processing), vol. 1. Berlin, Germany: Springer-Verlag, 2008.

[21] L. Harry and T. Van, *Optimum Array Processing*. Hoboken, NJ, USA: Wiley, 2002.

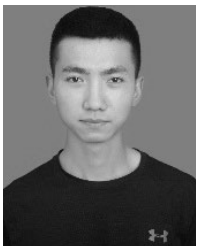

TIANYU CHEN received the B.S. degree in optoelectronics from the National University of Defense Technology (NUDT), Changsha, Hunan, China, in 2017, where he is currently pursuing the degree.

His current research interests include underwater DOA estimation and vector signal processing.

YANQUN WU was born in Shaowu, Fujian, China, in 1981. She received the B.S. and Ph.D. degrees in optical engineering from the National University of Defense Technology (NUDT), in 2004 and 2011, respectively.

Since 2011, she has been a Lecturer and then an Associate Professor with NUDT. In 2015, she was with SiPLAB, University of Algarve, Portugal, as a Visiting Scholar. Her current research interests include detection and estimation problems for both scalar and vector sensor array signal processing and underwater acoustics.

WEN ZHANG was born in Luotian, Hubei, China, in 1980. She received the B.S. degree in physics from Central China Normal University (CCNU), in 2003, the master's and Ph.D. degrees in optical engineering from the National University of Defense Technology (NUDT), in 2005 and 2012, respectively, and the joint Ph.D. degree from the University of Leeds, U.K., in 2010.

Since 2012, she has been a Lecturer with NUDT. Her current research interests include array signal processing and marine technology.

WEN CHEN received the B.S. degree in underwater acoustic engineering from Harbin Engineering University (HEU), Harbin, Heilongjiang, China, in 2017. She is currently pursuing the degree with the National University of Defense Technology (NUDT), Changsha, Hunan, China.

Her current research interests include underwater DOA estimation, interference suppression, and target tracking.

JUN WANG, photograph and biography not available at the time of publication.

ZHENGLIANG HU was born in Ningxiang, Hunan, China, in 1975. He received the B.S., master's, and Ph.D. degrees in optical engineering from the National University of Defense Technology (NUDT), in 1999, 2002, and 2005, respectively.

He is currently a Professor with NUDT. His current research interests include optic fiber sensors and marine science.